Inorganic Chemistry

ARTICLE

pubs.acs.org/IC

From Quantum Motifs to Assemble Nanoaggregates: The Preparation of Organo-Molybdenum Hybrid Nanostructures

Xiaoming Lu,* Xudong Shi, and Tao Min

Department of Chemistry, Capital Normal University, 100048 Beijing, China

Supporting Information

ABSTRACT: Nanoaggregates such as nanowires, nanoparticles, nanotubules, and nanoribbons were prepared from bulk crystals, which are shaped as needles (**1**), blocks (**2**), tubules (**3α**), and plates (**3*β***), respectively, by grinding and ultrasonication. Nanowires have diameters of approximately 2 nm, lengths of thousands of nanmeters, and the distance between adjacent nanowires is approximately 2 nm. The diameters of nanoparticles range from 3 to 5 nm. Nanotubules display diameters of 70 nm and lengths of thousands of nanometers, and nanoribbons exhibit widths of approximately 50 nm and lengths of hundreds of nanometers. All of the bulk crystals have been synthesized by the wet chemical method. Single-crystal X-ray diffraction reveals that crystal **1** is constituted by infinite one-dimensional $\{[NH_3CH_2CH(NH_2)CH_3](C_6H_4O_2)[\mu_2\text{-}OC_6H_4O](Mo^{VI}\text{-}O\text{-}Na\text{-}O)[NH_2CH_2CH(NH_2)CH_3]\}_n$ (**1**), which acts as a parallel aligned quantum wire forming lamellas that assemble themselves into multilayered architecture. Crystal **2** consists of discrete $[NH_3CH_2CH(NH_2)CH_3]_2[Mo^{VI}O_2(O_2C_6H_4)_2]$ (**2**), which presents as quantum particles and repeats itself along a three-dimensional crystal lattice. Crystal **3α**, formed under 5 °C, and **3*β***, crystallized above 10 °C, are both composed of $(NH_3CH_2CH_2NH_2)_2[Mo^{VI}O_2(O_2C_6H_4)_2](NH_2CH_2CH_2NH_2)_{0.5}$ (**3**) but are packed in different ways. In crystal **3α**, four $[Mo^{VI}O_2(O_2C_6H_4)_2]^{2-}$ circle into a quantum tube that is further assembled into multitubular architecture. However, in crystal **3*β***, two $[Mo^{VI}O_2(O_2C_6H_4)_2]^{2-}$ form a bilayered quantum lamellar motif that is piled into multilayered architecture. TEM reveals that all of the morphologies of the nanoaggregates are associated with the structures of the quantum motifs in their crystal lattices, which provide successful and effective access to assemble controlled nanostructures from quantum motifs of fine-desired and well-ordered bulk crystals. The technology of grinding and ultrasonication to prepare nanoaggregates is simple and available.

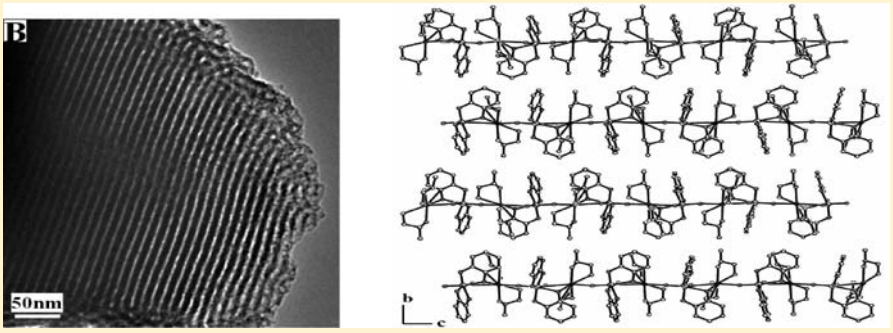

1. INTRODUCTION

Nanostructures, such as nanotubes, nanowires, nanorods, nanobelts, nanolamellas, and nanospheres, have been successfully synthesized.[1−13] How to assemble ordered nanoarchitecture has aroused extensive attention because of their potential application in materials and medicines.[14] Mo/W-based nanostructures are of special interest because of the key role of Mo/W in modern catalysis, magnetism, optics, and medical science.[15−19] At present, various methods, such as catalytic vapor−liquid−solid growth,[20] direct solid−solid and gas−solid reaction,[21] hydrothermal,[22] and template-based design techniques,[23] have been applied to assemble these architectures. However, the formation mechanisms of nanostructures still need to be clarified.[24] Here, we report a series of nanospecies that are prepared by grinding and sonication from a series of bulk crystals consisting of molybdenum-organic hybrids, $\{[NH_3CH_2CH(NH_2)CH_3](C_6H_4O_2)[\mu_2\text{-}OC_6H_4O](Mo^{VI}\text{-}O\text{-}Na\text{-}O)[NH_2CH_2CH(NH_2)CH_3]\}_n$ (**1**), $[NH_3CH_2CH(NH_2)CH_3]_2[Mo^{VI}O_2(O_2C_6H_4)_2]$ (**2**), and $(NH_3CH_2CH_2NH_2)_2[Mo^{VI}O_2(O_2C_6H_4)_2](NH_2CH_2CH_2NH_2)_{0.5}$ (**3**), and study the relationship between the structures of the motifs in the bulk crystals and the nanoaggregates of the motifs.

2. RESULTS AND DISSCUSSION

Zero Quantum Motif in Bulk Block Single Crystals and Its Nanoparticles. Panel (A) of Figure 1 displays the typical transmission electron microscope (TEM) images of a parallel alignment of nanowires that were prepared from bulk single crystal **1** by grinding and ultrasonication. The magnified images (Figure 1B, C) show the perfect assembly of the nanowires with diameters of approximately 2 nm, lengths of thousands of nanometers, and distances of about 2 nm between adjacent nanowires.

The single-crystal X-ray analysis reveals that crystal **1** (orthorhombic, space group *Pbca*) consists of complex $\{[NH_3CH_2CH(NH_2)CH_3](C_6H_4O_2)(\mu_2\text{-}OC_6H_4O](Mo\text{-}O\text{-}Na\text{-}O)[NH_2CH_2CH(NH_2)CH_3]\}_n$ (**1**) with an infinite coordinated one-dimensional structure along the *c* axis (Figure 1D). In complex

Received: August 7, 2010
Published: February 14, 2011

dx.doi.org/10.1021/ic101597q | *Inorg. Chem.* 2011, 50, 2175–2181

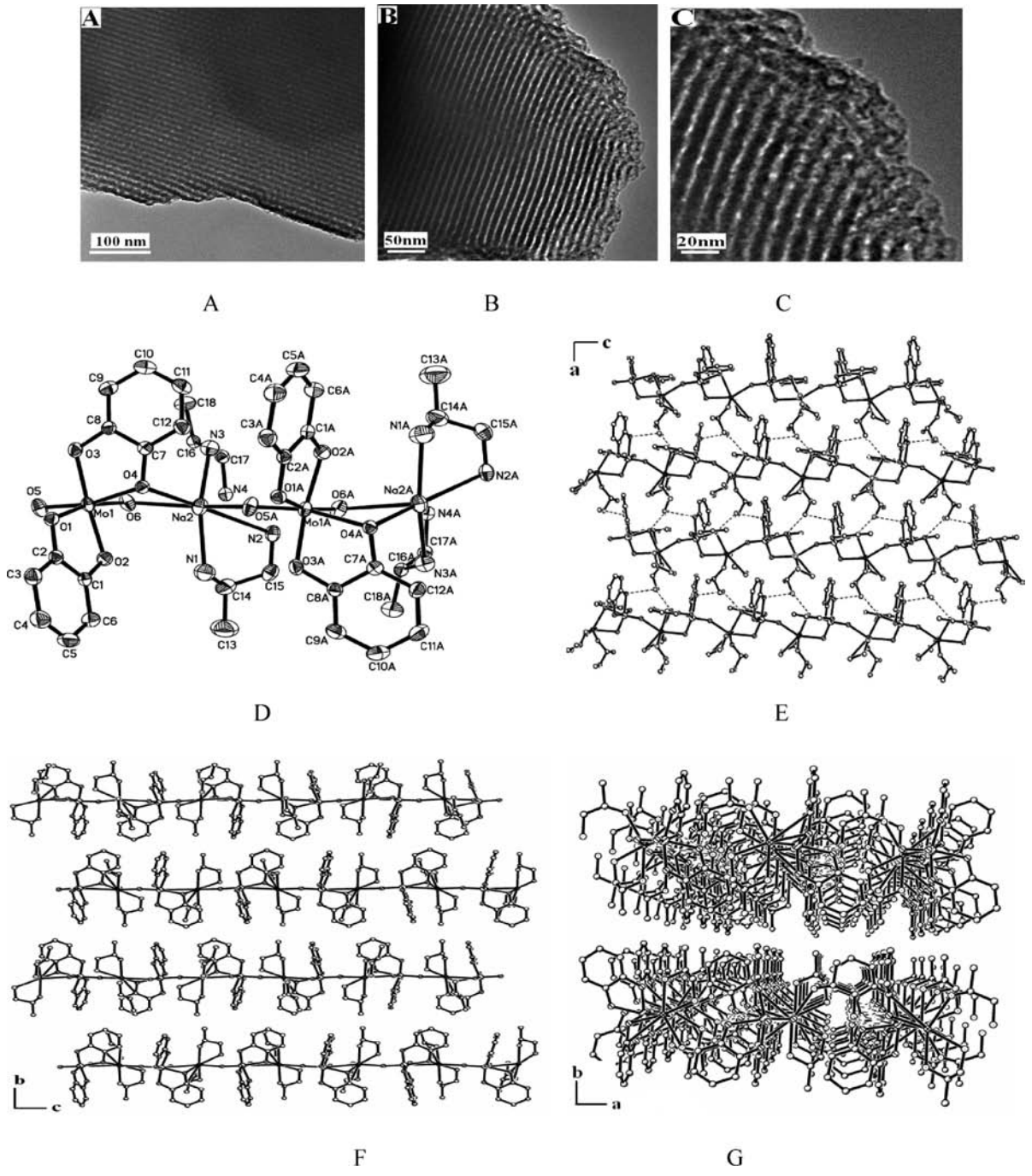

Figure 1. Nanowires (A, B, and C; scale bars are 100, 50, and 20 nm, respectively). The molecular structure of complex **1** with 30% probability displacement ellipsoids with hydrogen atoms is omitted for clarity (D), and its packing along the *b* (E), *a* (F), and *c* axis (G).

1, every Mo (Mo1) coordinates with four O (O1, O2, O3, and O4) atoms from two pyrocatechol ligands and two O_t (O5 and O6) atoms that act as a bibridge link with Na, respectively. O2 and O3 coordinate with Mo1 in *trans*-position, and O1 connects with Mo1 in *cis*-position, whereas O4 acts as a tribridge connecting with Mo1 (in *cis*-position), Na2, and C7 atoms. The Mo−O_t bond lengths are 1.715 (3) and 1.722 (3) Å. The Mo−O_{trans} bond lengths are 1.996 (3) and 1.981 (3) Å. The Mo−O1 bond length is 2.136(2) Å, and the Mo−O4 bond length is 2.175(2) Å. The O5−Mo−O6 bond angle is 103.6 (2)°, and the O6−Na2−O5A bond angle is 151.4 (0)°. The Na, eg., Na2, not only connects with O4, O5A, and O6 atoms, but also coordinates with three N (N1, N2, and N3) atoms. N1 and N2 from a neutral 1,2-DAP constitute a (N−C−C−N−Na) five-membered ring with Na−N bond lengths of 2.372 (6) and 2.829 (4) Å. N3 is from another protonated 1,2-DAP with a Na−N bond length of 2.462(4) Å. The protonated 1,2-DAP, as a bridge, links to two O_{trans} atoms from an adjacent chain, with N4−H···O1A(O3A) with a length of 1.983 Å, forming lamellar structure (Figure 1E). The lamella piles up forming a multilayer architecture along the *b* axis (Figure 1F, G).

The most striking structural feature of crystal **1** is the infinite one-dimensional complex **1**, which acts as quantum motif and

dx.doi.org/10.1021/ic101597q |*Inorg. Chem.* 2011, 50, 2175–2181

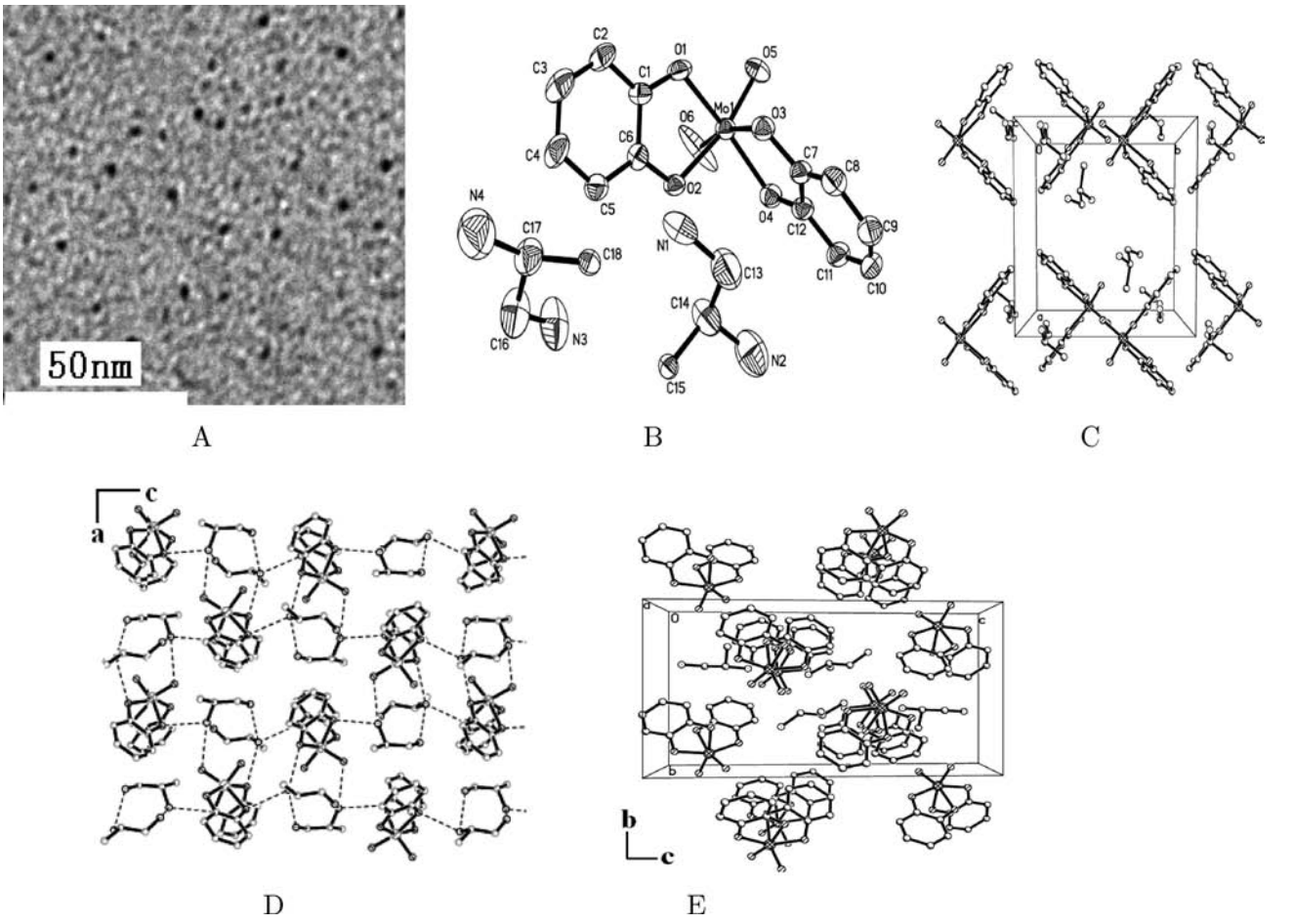

Figure 2. (A) Nanoparticle (scale bar 50 nm) molecular structure of complex **2**, with 30% probability displacement ellipsoids, with hydrogen atoms omitted for clarity. (B) Couple of enantiomers and its packing diagram along the *c* axis (C). Ten-membered ring and its packing diagram along the *b* axis (D) and its packing diagram along the *a* axis (E).

parallel alignes into quantum lamella in the *ac* plane by geometry insertion and hydrogen bonds (Figure 1E), and the lamellas pile into multilayered architecture along the *b* axis through the Van der waals force (Figure 1F, G). Similar to graphite, the Van der waals force between lamellas is easy to break, so that the multilayered structure slips easily into monolayers or nanolamellas, which are constituted by the parallel alignment of the nanowires.[25,26] As deduced above, after crystal **1** was ground into a fine powder with agate mortar, the powder was mixed with ether, and the mixture was ultrasonicated with ultrasonication cleaner. The nanowire array is shown under TEM (Figure 1A, B, C), which is similar to the parallel alignment of the 1-D chain structure in the crystal lattice of complex **1** (Figure 1F). However, the nanowire array can not be obtained if the fine powder is not treated by ultrasonocation.

In ultrasonication, the ultrasonic wave can cause a large number of microbubbles form, grow, and collapse in a very short time; this is called ultrasonic cavitation.[27] The cavitation can generate local temperatures as high as 5000 K and local pressures as high as 500 atm, with heating and cooling rates greater than 109 K/s.[28] The production of the nanowires illustrates that the weak Van der waals forces between adjacent lamellas along the *b* axis in crystal **1** can be broken, and the multilamellar structure can slip into single lamella, which assembles the parallel-aligned nanowires by ultrasonic cavitation. It also provides a new method to prepare nanowires; that is synthesizing an infinite one-dimensional structure molecule as quantum wires, aligning them parallel into lamellas through geometrical insertions, linking the lamellas into multilayered bulk single crystals through a weak Van der waals force, grinding the crystals into fine powder with an agate mortar, ultrasonicating the powder in unsolved liquid and breaking the weak interaction between the lamellas, and obtaining nanowire. It worth noting that there is a correlation between the quantum motif in bulk single crystals and their nanoaggregate in the powder state, e.g., the nanowire is similar to the quantum wire.

Zero Quantum Motif in Bulk Block Single Crystals and Its Nanoparticles. To study the relationship of quantum motifs in bulk crystals and their nanoaggregate in the powder state, the reactant $[(CH_3CH_2CH_2CH_2)_4N]_4Mo_8O_{26}$ was used to replace $Na_2MoO_4 \cdot 2H_2O$, and bulk single crystal **2** with block morphology was synthesized. Nanoparticles (Figure 2A) were prepared from crystal **2** by grinding and ultrasonication.

In contrast to the infinite one-dimensional complex **1**, the X-ray crystal structural analysis reveals that crystal **2** (monoclinic, space group $P2_1/n$) consists of discrete complex **2** $[NH_3CH_2CH(NH_2)CH_3]_2[Mo^{VI}O_2(O_2C_6H_4)_2]$, which acts as a zero-dimensional quantum motif in crystal lattices. In complex **2**, each Mo coordinates with two catechol ligands, displaying a *cis*-dioxo fashion with a chiral pseudo-octahedral $[MO_6]$ coordination

dx.doi.org/10.1021/ic101597q |*Inorg. Chem.* 2011, 50, 2175–2181

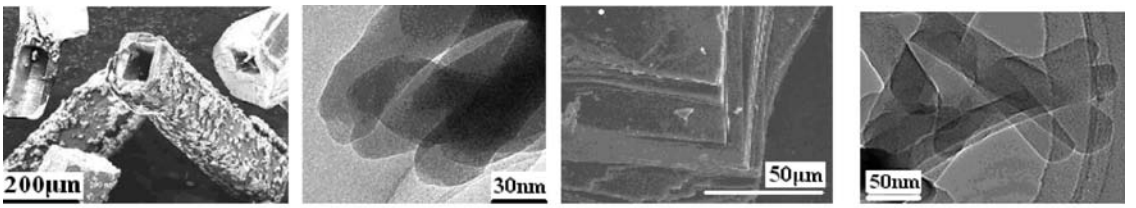

Figure 3. SEM images of bulk tubular crystals (A) and lamellar crystals (C); scale bar is 200 and 50 μm, respectively. TEM images of nanotubules (B) and nanoribbons (D); scale bar is 30 and 50 nm, respectively.

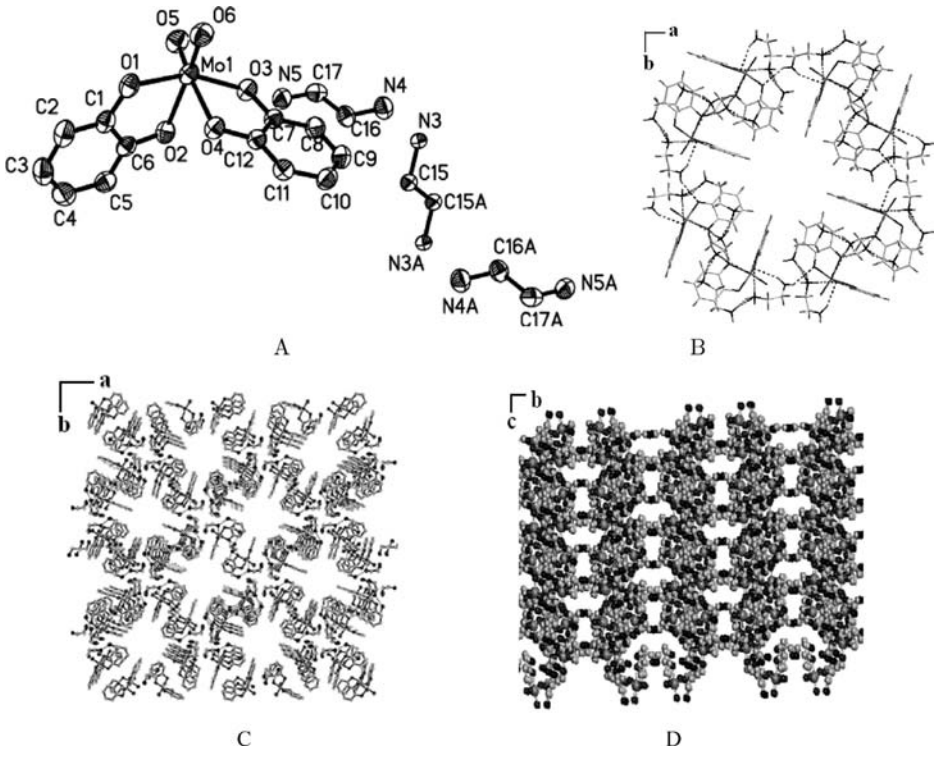

Figure 4. Molecular structure of complex **3** with 30% probability displacement ellipsoids with hydrogen atoms omitted for clarity (A), their packing diagram in the *ab* plan (B and C), along the *a* axis (D) in crystal **3α**.

geometry (Figure 2B). The chiral anion $[Mo^{VI}O_2(OC_6H_4O)_2]^{2-}$ exhibites two types of enantiomeric structures (lambda/delta configuration), and the two enantiomers couple with each other (Figure 2C). Each $[Mo^{VI}O_2(O_2C_6H_4)_2]^{2-}$ is surrounded by six (H−N−C−C−N···H−N−C−C-N···) ten-membered ring units through hydrogen bonds along the *a*, *b*, and *c* axis (Figure 2E, D, C, respectively). The ten-membered ring is formed by a enantiomeric cation $[NH_3CH_2CH(NH_2)CH_3]^+$ coupled with its mirror image. Likewise, every ten-membered ring is surrounded by six $[Mo^{VI}O_2(O_2C_6H_4)_2]^{2-}$ anions through Mo−O4···H-N3 hydrogen bonds along the *a*, *b*, and *c* axis. Because the hydrogen bonds are unstable, the $[NH_3CH_2CH(NH_2)CH_3]^+$ cations are easily neutralized by devoting a H^+ to $[Mo^{VI}O_2(O_2C_6H_4)_2]^{2-}$, which can accept one or two H^+, becoming $[Mo^{VI}(OH)O(O_2C_6H_4)_2]^-$ or $[Mo^{VI}(OH)_2(OC_6H_4O)_2]$. The neutralized $CH_2NH_2CH(NH_2)CH_3$ is volatile at room temperature. Therefore, it is inferred that the hydrogen bonds of crystal **2** could be broken up, and the $CH_2NH_2CH(NH_2)CH_3$ could be evaporated and escaped under ultrasonicate cavitation[29] so that the bulk block single crystal **2** could be disassembled into discrete nanoparticles, which assemble by the zero-dimensional quantum motif.

As expected, when bulk block crystal **2** was ground into fine powder with agate mortar, the powder was put into ether then treated by sonication with an ultrasonic cleaner; after 1 h, the nano particles with diameters between 3 and 5 nm were observed under TEM (Figure 2A). However, the nanoparticles cannot be obtained if the fine powder is not treated by ultrasonocation. The result shows that the weak interaction among quantum motifs can be broken up by grinding and ultrasonication, and the bulk single crystals can be disassembled into nanoparticles. It is needed to clarify that not all the Mo−O···H-N bonds were transferred into Mo−OH and all the $(CH_2NH_2CHCH_2NH_3)^+$ cations were neutralized; the $[Mo^{VI}O_2(O_2C_6H_4)_2]^{2-}$ anions and $(CH_2NH_2CHCH_2NH_3)^+$ cations within the nanoparticles still exist and are well-ordered the same as they are in bulk single crystals. Of course, this deduction needs to be confirmed further by finer techniques.

Tubular Quantum Motif in Bulk Tubular Single Crystals and Its Nanotubules and Lamella Quantum Motif in Bulk Lamellar Single Crystals and Its Nanoribbons. Furthermore, $(NH_3CH_2CH_2NH_2)^+$ was used instead of $(NH_3CH_2CHNH_2CH_3)^+$, and bulk tubular crystal **3α** (Figure.3A) and bulk plate

dx.doi.org/10.1021/ic101597q |*Inorg. Chem.* 2011, 50, 2175–2181

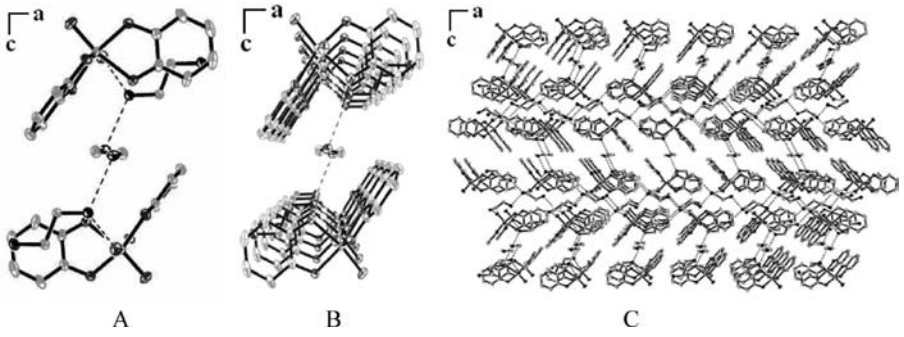

Figure 5. Packing diagram of complex **3** in the *ac* plan in crystal **3*β***.

crystal **3*β*** (Figure 3C) were obtained. Crystal **3α** formed under 5 °C, and crystal **3*β*** was produced above 10 °C. Both of them are composites of $(NH_3CH_2CH_2NH_2)_2[Mo^{VI}O_2(O_2C_6H_4)_2](NH_2CH_2CH_2NH_2)_{0.5}$ (**3**). From crystals **3α** and **3*β***, nanotubules (Figure 3B) and nanoribbons (Figure 3D) were prepared separately by grinding and ultrasonication and were observed under TEM.

The X-ray crystal structural analysis reveals that crystal **3α** with a bulk tubular crystal structure is tetragonal with space group $P4_2/n$, $a = 25.214(8)$ Å, $c = 7.484(4)$ Å, and $Z = 8$. The Mo center coordinates with two catechol ligands, displaying a *cis*-dioxo fashion with chiral pseudo-octahedral $[MO_6]$ coordination geometry (Figure 4A). However, in contrast to complex **1** and **2**, the chiral anion $[Mo^{VI}O_2(O_2C_6H_4)_2]^{2-}$ combine with two protonated $(NH_3CH_2CH_2NH_2)^+$ cations and a half neutral $NH_2CH_2CH_2NH_2$ molecule. In crystal lattices, each line of chiral anion $[Mo^{VI}O_2(O_2C_6H_4)_2]^{2-}$ is in the same enantiomeric configuration (lambda/delta) along the *c* axis and couple with their adjacent mirror image configuration (delta/lambda) in the *ab* plane. Four pairs of enatiomeric chains are linked by protonated $(NH_3CH_2CH_2NH_2)^+$ cations and a neutral $NH_2CH_2CH_2NH_2$ through hydrogen bonds, forming a square tubular structure with an open channel of 7.06 × 7.06 Å in the *ab* plane (Figure4B), which as a quantum motif assembles a multitubular framework with intervals of 7.75 × 7.75 Å among the square tubules (Figure 4C). Similar to crystal **2**, the protonated $(NH_3CH_2CH_2NH_2)^+$ cation is easily neutralized and escapes under grinding and ultrasonication. Cation $[Mo^{VI}O_2(O_2C_6H_4)_2]^{2-}$ can be protonated at the terminal O atoms, so it is inferred that the multitubular framework could also be broken into nanotubules due to evaporation of $NH_2CH_2CH_2NH_2$ and the broken hydrogen bonds among the $[Mo^{VI}O_2(O_2C_6H_4)_2]^{2-}$ and $(NH_3CH_2CH_2NH_2)^+$ cations.

As expected, when bulk crystal **3α** was ground into fine powder, the powder was put into ether, and the mixture was treated by sonication with an ultrasonic cleaner. Then the nanotubules with an internal diameter of about 50 nm were observed under TEM (Figure 3B). It is worth noting that the nanotubular morphology is similar to that of the quantum tubular motifs of crystal **3α** (Figure 4B, C, D), though the relationship between the scale of the nanotubules and that of the quantum motif needs further study.[30]

In contrast, the X-ray crystal structural analysis reveals that bulk lamellar crystal **3*β*** is monoclinic with space group $P2_1/c$, $a = 7.1254(2)$ Å, $b = 30.7496(9)$ Å, $c = 9.7857(3)$ Å, $\beta = 102.411(2)°$, and $Z = 4$. Crystal **3*β*** is also composed of one *cis*-dioxomolybdenum center $[Mo^{VI}O_2(O_2C_6H_4)_2]^{2-}$ and two $(NH_3CH_2CH_2NH_2)^+$ counterions and a half neutral $NH_2CH_2CH_2NH_2$ molecule (Figure 5A). The difference between crystals **3*β*** and **3α** is the packing style of the complex **3** in the crystal lattice. In crystal **3*β***, each chiral $[Mo^{VI}O_2(O_2C_6H_4)_2]^{2-}$ coupled with its enantiomer is linked by $(NH_3CH_2CH_2NH_2)^+$ and neutral $NH_2CH_2CH_2NH_2$ through hydrogen bonds along the *c* axis (Figure 5A). The pairs of enantiomers are packed through $\pi-\pi$ interaction along the *b* axis (Figure 5B) and through molecular interactions along *a* axis in the same configuration (Figure.5C). That is, each line of the molecules is in the same enantiomeric configuration along the *a* axis and *b* axis, while in the mirror image configuration along the *c* axis, which constitutes a bilayered structure as a quantum motif. The quantum motif piles into a multilayered lamellar structure along the *c* axis linked by a hydrogen bond. Similar to the crystals above, the weak interactions, eg., hydrogen bonds and Van der waals forces, are unstable under grinding and ultrasonication, and the protonated $(NH_3CH_2CH_2NH_2)^+$ cation is easily neutralized and escapes, so it is possible that the multilamellar framework slips into nanolamellas and breaks further into nanoribbons.

As expected, when bulk crystal **3*β*** was ground into fine powder, the powder was mixed with ether, and the mixture was treated by sonication with an ultrasonic cleaner. The nanoribbons, with widths and lengths of about 30 nm and hundreds of nanometers, respectively, were observed under TEM (Figure 3D), though the relationship between the scale of the nanoribbons and the multilayered lamellar structure needs studied further.

3. EXPERIMENTAL SECTION

3.1. Materials and Measurements. All reagents were directly obtained from commercial supplies with analytical grade. All manipulations were carried out in the laboratory atmosphere. Single-crystal structure determination was performed on a Bruker APEXII area detector device with Mo Kα radiation ($\lambda = 0.71073$ Å) by the $\Phi-\omega$ scan method. The transmission electron microscopy (TEM) experiments were recorded on a Tecnai 20 G2 S-TWIN electron microscopy.

3.2. Synthesis of Bulk Single Crystals. *Crystal* ***1***. Ten mmoL of pyrocatechol, 1 mmoL of $Na_2MoO_4 \cdot 2H_2O$, and 8 mL of $NH_2CH_2CH(NH_2)CH_3$ were added to a mixed solvent of CH_3OH (15 mL) and CH_3CN (15 mL) at room temperature, forming a dark-red solution, then changing to yellow immediately. After 6 h, the mother solution was filtered into a tube, and the filtrate was layered with Et_2O. Two weeks later, red needle-shaped single crystals were obtained. Elem. Anal. Calcd: C 41.86%, H 5.62%, N 10.86%. Found (before grinding and sonication): C 41.96%; H 5.57%; N 10.79%. Found (after grinding and

dx.doi.org/10.1021/ic101597q |*Inorg. Chem.* 2011, 50, 2175–2181

sonication): C 41.96%; H 5.57%; N 10.78%. IR spectrum (KBr, cm^{-1}): ν_s(N−H) 3413.58$_m$, ν_s(C−H) 2980.89$_m$, ν_s(C═C) 1602.14$_m$, 1479$_s$, ν_s(C−O) 1253$_s$, ν_s(Mo═O) 962.94$_s$, ν_s-(Mo−O) 872.37$_s$. ^{1}H NMR spectra of complex **1** show five sets of peaks according to ArH, $-CH_3$, $-CH_a(H_b)$, and $-CH_x$. Because of the chirality C* atom in $CH_a(H_b)(NH_2)C^*H_x$-$(NH_2)CH_3$, the H_a and H_b, which form an ABX system with H_x, are nonequivalent chemically and magnetically. ^{13}C NMR spectra of the complex show four sets of peaks. NMR data in D_2O: ($\{[NH_3CH_a(H_b)C^*H_x(NH_2)CH_3](C_6H_4O_2)[\mu_2$-$OC_6$-$H_4O](Mo$-O-Na-O$)[NH_2CH_a(H_b)C^*H_x(NH_2)CH_3]\}_n$). ^{1}H: δ 6.623−6.705 (m, ArH), 3.100 (m, CH_x), 2.746 (m, CH_a), 2.686 (m, CH_b), 1.136 (d, CH_3). ^{13}C: δ 116.236−158.260 (ArC), 50.038 (CH), 48.640 (CH_2), 20.513 (CH_3).

Crystal ***2***. $[(n\text{-}Bu)_4N]_4[Mo_8O_{26}]$ (5 mmol) and catechol (10 mmol) were dissolved in a mixed solvent of CH_3OH (15 mL) and CH_3CN (15 mL). Then $CH_3CHNH_2CH_2NH_2$ (5 mL) was added, and the solution was filtrated after 6 h of stirring. The red filtrate was layered with ether for two weeks under 5 °C, and red block-like crystals were obtained. Elem. Anal. Calcd: C 43.64%, H 6.26%, N 11.30%. Found (before grinding and sonication): C 43.66%; H 6.23%; N 11.33%. Found (after grinding and sonication): C 41.83%; H 5.11%; N 9.02%. IR spectrum (KBr, cm^{-1}): ν_s(N−H) 3435$_m$, ν_s(C−H) 2957$_m$, ν_s(C═C) 1603$_m$, 1478$_s$, ν_s(C−O) 1258$_s$, ν_s(Mo═O) 899$_s$, ν_s(Mo−O) 872$_s$. ^{1}H NMR in D_2O solution, δ 6.59−6.73 (m, ArH), 3.29 (m, CH), 2.903 (dd, CH_b), 2.86 (dd, CH_a), 1.23 (d, CH_3).

Crystal ***3α***. $[(n\text{-}Bu)_4N]_4[Mo_8O_{26}]$ (5 mmol) and catechol (10 mmol) were dissolved in a mixed solvent of CH_3OH (15 mL) and CH_3CN (15 mL). Then $NH_2CH_2CH_2NH_2$ (5 mL) was added, and the solution was filtrated after 6 h of stirring. The red filtrate was layered with ether for two weeks under 5 °C, and red tubular-like crystals were obtained. Elem. Anal. Calcd: C 41.05%, H 6.28%, N 14.08%. Found (before grinding and sonication): C 41.37%; H 6.45%; N 14.81%. Found (after granding and sonication): C 40.12%; H 4.26%; N 12.90%. IR spectrum (KBr, cm^{-1}): ν_s(N−H) 3435$_m$, ν_s(C−H) 2957$_m$, ν_s(C═C) 1603$_m$, 1478$_s$, ν_s(C−O) 1253$_s$, ν_s(Mo═O) 899$_s$, ν_s(Mo−O) 872$_s$. ^{1}H NMR in D_2O solution, δ 6.49 (m, ArH), 2.75 (s, CH_2). ^{13}C NMR of solid state, δ 158.5(*ipso*-C), 157.7 (*ipso*-C), 123.3 (Ar−C), 120.4 (Ar−C), 117.6 (Ar−C), 115.0 (Ar−C), 41.6 (CH_2).

Crystal ***3β***. $[(n\text{-}Bu_4)N]_4[Mo_8O_{26}]$(5 mmol) and catechol (10 mmol) were dissolved in a mixed solvent of CH_3OH(15 mL) and CH_3CN(15 mL). Then $NH_2CH_2CH_2NH_2$(5 mL) was added, and the solution was filtrated after 6 h of stirring. The red filtrate was layered with ether for two weeks above 10 °C, and red lamellar-like crystals were obtained. Elem. Anal.Calcd: C 41.00; H 6.69; N 15.93. Found (before grinding and sonication): C 41.21; H 6.65; N 15.72. Found (after grinding and sonication): C 39.10%; H 2.88%; N 11.56%. IR spectrum (KBr, cm^{-1}): ν_s(N−H) 3435$_m$, ν_s(C−H) 2957$_m$, ν_s(C═C) 1603$_m$, 1478$_s$, ν_s(C−O) 1253$_s$, ν_s(Mo═O) 899$_s$, ν_s(Mo−O) 872$_s$. NMR in D_2O: ^{1}H NMR in solution, δ 6.46(m, Ar−H), 4.60, 2.71(s, CH_2). ^{13}C NMR in solution, δ 154.31 (*ipso*-C), 118.74 (Ar−C), 114.81 (Ar−C), 112.29 (Ar−C), 38.64 (CH_2); ^{13}C NMR of solid state, δ= 157.7 (*ipso*-C), 123.8 (Ar−C), 122.6 (Ar−C), 116.5 (Ar−C), 115.4 (Ar−C), 44.7 (CH_2), 43.1 (CH_2), 40.3 (CH_2), 38.7 (CH_2).

3.3. X-ray Crystallography. The crystal structure was solved by direct methods with SHELXS-97.[31] An absorption correction based on symmetry-equivalent reflections was applied by using the SADABS program.[32] The final refinement included atomic positions for all the atoms and anisotropic thermal parameters for all the non-hydrogen atoms. Full-matrix least-squares structure refinement against $|F^2|$ was carried out with the SHELXTL-PLUS package programs.[33] CCDC-292615 for crystal **1**, CCDC-294700 for crystal **2**, CCDC-272632 for crystal **3α**, and CCDC 270004 for crystal **3*β*** contains the supplementary crystallographic data for this paper, which can be obtained from www.ccdc.cam.ac.uk/conts/retrieving.html (or from Cambridge Crystallographic Data Centre, 12 Union Road, Cambridge CB21EZ (Fax: 0044−1223−336−033 or e-mail: deposit@ccdc.cam.ac.uk).

Pertinent experimental details for the structure determination are presented in Table 1 of the Supporting Information. The crystallographic data and collection parameter of crystals **1**, **2**, **3α**, and **3*β*** are shown in Table 1 of the Supporting Information, and the selected bond lengths and angles of the four crystals are presented in Table 2 of the Supporting Information.

3.4. Preparation of the Nanostructures. Bulk single crystals **1**, **2**, **3α**, and **3*β*** were ground into fine powder separately, and the powders were put into ether. The mixtures were treated by sonication with an ultrasonic cleaner under 40 kHz at room temperature. After 1 h sonication, the product was checked under TEM.

4. CONCLUSIONS

Needle crystal **1**, block crystal **2**, tubular crystal **3α**, and plate crystal **3*β*** have been synthesized by a wet chemical method, and nanoaggregates that are nanowires, nanoparticles, nanotubules, and nanoribbons were prepared from crystals **1**, **2**, **3α**, and **3*β***, respectively, by grinding and ultrasonication. Single-crystal X-ray diffraction reveals that crystal **1** is constituted by infinite one-dimensional $\{[NH_3CH_2CH(NH_2)CH_3](C_6H_4O_2)[\mu_2$-$OC_6H_4O]$-$(Mo^{VI}$-O-Na-O$)[NH_2CH_2CH(NH_2)CH_3]\}_n$ (**1**), which acts as a quantum wire parallel aligned, forming lamellas that assemble themselves into multilayered architecture. Crystal **2** consists of discrete $[NH_3CH_2CH(NH_2)CH_3]_2[Mo^{VI}O_2(O_2C_6H_4)_2]$ (**2**), which presents as quantum particles that repeat themselves along three-dimensions in the crystal lattice. Both crystals **3α**, formed under 5 °C, and crystal **3*β***, crystallized above 10 °C, are composed of $(NH_3CH_2CH_2NH_2)_2[Mo^{VI}O_2(O_2C_6H_4)_2](NH_2$-$CH_2CH_2NH_2)_{0.5}$ (**3**) but are packed in different ways. In crystal **3α**, four $[Mo^{VI}O_2(O_2C_6H_4)_2]^{2-}$ circles into quantum tubular motifs, which assemble themselves into multitubular architecture. However, in crystal **3*β***, two $[Mo^{VI}O_2(O_2C_6H_4)_2]^{2-}$ couple into bilayered quantum lamellar motifs, which pile themselves into multilayered architecture. TEM reveals that the nanowires have diameters of about 2 nm, lengths over thousands of nanometers, and the distance between adjacent nanowires is about 2 nm. The nanoparticles exhibit diameters from 3 to 5 nm. The nanotubules present diameters about 70 nm and lengths over thousands of nanometers; and the nanoribbons display widths of about 50 nm and lengths over hundreds of nanometers. It is worth noting that all of the morphologies of the nanoaggregates are associated with the structures of the quantum motifs in their crystal lattices. The nanowires are almost the same as the quantum wire motif. The nanoparticles are similar to the quantum particle motif. The nanotubules are associated with the quantum tubule motif, and the nanoribbon is formed by the breaking of quantum lamella, which provides successful and effective access to assemble controlled nanostructures from quantum motifs of fine-desired and well-ordered bulk crystals. It is worth noting also that

preparing nanoaggregates by grinding and ultrasonication is rather moderate and available, which is much easer, more inexpensive, and safer to process than other methods in the laboratory, and is especially useful for organo-metallic hybrids that could be destroyed by other technology.

■ ASSOCIATED CONTENT

Supporting Information. Crystallographic datas for crystals 1, 2, 3α and 3β; selected bond distances (Å) and angles (°) for crystals 1, 2, 3α and 3β; and XPS spectras. This material is available free of charge via the Internet at http://pubs.acs.org.

■ AUTHOR INFORMATION

Corresponding Author
*E-mail: lu-xiaoming@126.com.

■ ACKNOWLEDGMENT

We acknowledge the financial support of the Chinese National Natural Science Foundation (20871085) and Beijing Natural Science Foundation (2092009).

■ REFERENCES

(1) Alivisatos, A. P. *Science* **1996**, *271*, 933.
(2) Yakobson, B. I.; Smalley, R. E. *Am . Sci.* **1997**, *85*, 324.
(3) Tenne, R.; Margulis, L.; Genut, M.; Hodes, G. *Nature* **1992**, *360*, 444.
(4) Yada, M.; Mihara, M.; Mouri, S.; Kuroki, M.; Kijima, T. *Adv. Mater.* **2002**, *14*, 309.
(5) Ma, R. Z.; Bando, Y.; Zhang, L. Q.; Sasaki, T. *Adv. Mater.* **2004**, *16*, 918.
(6) Siddhartha, S.; Tanmay, B.; Sunil, K. S.; Gajendra, S.; Ramachandrarao, P.; Debabrata, D. *ACS Nano* **2009**, *3*, 1357.
(7) Anil, K.; Yuko, I.; Mitsunori, Y.; Kenichi, N. *J. Am. Chem. Soc.* **2007**, *129*, 1534.
(8) Steven, D. P.; Warren, C. W. C *J. Am. Chem. Soc.* **2009**, *131*, 17042.
(9) Dai, H. J.; Wong, E. W.; Lu, Y. Z.; Fan, S. S.; Lieber, C. M. *Nature* **1995**, *375*, 769.
(10) Jung, H. Y.; Jin, J.; Hyun, M. P.; Sung, B.; Young, W. K; Sung, C. K.; Taeghwan, H. *J. Am. Chem. Soc.* **2005**, *127*, 5662.
(11) Pan, Z. W.; Dai, Z. R.; Ma, C.; Wang, Z. L. *J. Am. Chem. Soc.* **2002**, *124*, 1817.
(12) Pei, Y. K.; Bo, Y. K.; In-Bo, S.; Rabindra, S.; Peter, E. V.; Neal., R. A.; Heemin, Y. *ACS Nano* **2009**, *3*, 3143.
(13) Paritosh, M.; Ilsun, Y.; Taejoon, K.; Kwanyong, S. *J. Am. Chem. Soc.* **2007**, *129*, 9576.
(14) Braun, P. V.; Osener, P.; Stupp, S. I. *Nature* **1996**, *380*, 325.
(15) Vivek, P.; Babita, B.; Rajender, S. V. *ACS Nano* **2009**, *3*, 728.
(16) Li, Y.; Zhou, Z.; Zhang, S.; Chen, Z. *J. Am. Chem. Soc.* **2008**, *130*, 16739.
(17) Ding, Y.; Wan, Y.; Min, Y.-L.; Zhang, W.; Yu, S.-H. *Inorg. Chem.* **2008**, *4*, 7813.
(18) Fiorenzo, V.; Fabio, V.; Paulo, T. O.; Sylvia, F. Z.; Yi, J.-H.; Johannes, S. *Nano Lett.* **2009**, *9*, 659.
(19) Zhang, J.; Soon, J. M.; Lon, K. P. *Nano Lett.* **2007**, *7*, 2370.
(20) Kiely., C. J.; Fink, J.; Brust, M.; Bethell, D.; Schiffrin, D. J. *Nature* **1998**, *396*, 444.
(21) Penn., R. L.; Banfield, J. F. *Science* **1998**, *281*, 969.
(22) Lou, X. W.; Zeng, H. C. *Chem. Mater .* **2002**, *14*, 4781.
(23) Cui, Y.; Lieber, C. M. *Science* **2001**, *291*, 851.
(24) Puntes., V. F.; Krishnan, K. M.; Alivisatos, A. P. *Science* **2001**, *291*, 2115.
(25) Tang., Z. Y.; Kotov, N. A.; Giersig, M. *Science* **2002**, *297*, 237.
(26) Gao, P. X.; Ding, Y.; Wang, Z. L. *Nano Lett.* **2003**, *3*, 1315.
(27) Lao, J. Y.; Huang, J. Y.; Wang, D. Z.; Ren, Z. F. *Nano Lett,.* **2003**, *3*, 235.
(28) Li, J.; Papadopoulos, C.; Xu, J. M. *Nature* **1999**, *402*, 253.
(29) Tang, E. S. K.; Huang, M.; Lim, L. Y. *Int. J. Pharm.* **2003**, *265*, 103.
(30) Lu, X. F.; Mao, H.; Chao, D. M. *J. Solid State Chem.* **2006**, *179*, 2609.
(31) Sheldrick, G. M. *SHELXTL-97*, V5.10; Bruker AXS Inc.: Madison, WI, 1997.
(32) Sheldrick, G. M. *SADABS, Program for Empirical Absorption Correction of Area Detector Data*; University of Gottingen, Gottingen, Germany, 1996.
(33) Sheldrick, G. M. *SHELXTL-Plus*; Madison, WI, 1990.